

Structure and Vibrational Spectra of the Zwitterion L-Alanine in the Presence of Explicit Water Molecules: A Density Functional Analysis

Emadeddin Tajkhorshid,[§] K. J. Jalkanen, and Sándor Suhai*

Department of Molecular Biophysics, German Cancer Research Center, Im Neuenheimer Feld 280, D-69120 Heidelberg, Germany

Received: November 24, 1997; In Final Form: March 6, 1998

Ab initio B3LYP/6-31G* optimized geometries, vibrational frequencies, and absorption intensities have been calculated for the L-alanine zwitterion (ALAZW) structures stabilized by four neighboring water molecules. The ALAZW structures were stabilized by the addition of four neighboring water molecules because at the B3LYP/6-31G* level of theory the ALAZW is not stable in the absence of the water molecules and will be converted to the nonionized species. The ALAZW was not stable at this level of theory within the Onsager continuum model using the recommended cavity radius obtained from the solute volume calculations. Geometry optimization of the ALAZW in the presence of the explicit water molecules resulted in different optimized structures for the amino acid itself. The distributed origin gauge atomic axial tensors and the electric dipole–electric dipole polarizability derivatives calculated at the RHF level of theory were combined with the B3LYP normal modes, frequencies, and atomic polar tensors to calculate the vibrational absorption, the vibrational circular dichroism, and polarized Raman scattering intensities for the ALAZW structures. These calculated vibrational spectra of the solute were found to be very sensitive to the relative arrangement of the neighboring water molecules.

Introduction

Determination of the conformational details of biological macromolecules is important to understand their functions. The relevance of the molecular structures in the crystalline phase for biological molecules in aqueous solution is often questioned. With this regard experimental approaches such as NMR and Raman spectroscopy allow us to get structural and electronic information on these molecules in aqueous solution which complements the information obtained from crystallography studies. Because of the complexity of the spectra, theoretical studies are used to identify and interpret the vibrational modes. However, since it is difficult to implement this approach directly for large systems such as proteins, model systems have to be studied first to understand the properties of the building units, such as amino acids. The conformational flexibility of amino acids, established both experimentally^{1–6} and theoretically,^{7–17} can be influenced by the presence of solvent molecules through electrostatic interactions and hydrogen bond formation.

Alanine is the smallest naturally occurring chiral amino acid. In peptides and proteins the conformational properties of many other residues may be well modeled by this simple molecule. The dominant species of alanine in aqueous solution is the zwitterionic form, an asymmetric structure with a chiral center to which locally symmetric groups are attached (Figure 1). There have been a number of nonempirical theoretical studies on the structure of alanine.^{12,17–21} In many studies the amino acid has been treated in the nonionized form.^{12,17–19} This consideration, however, may be insufficient for the complete description of the molecule in aqueous solution. It is well known that amino

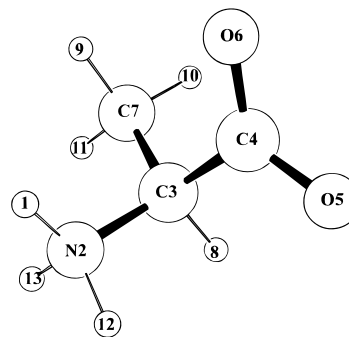


Figure 1. Schematic presentation of ALAZW and the atom numbering which has been used in order to report the geometries and to determine the normal coordinates. The atom types are only shown for heavy atoms.

acids exist as zwitterions in the crystalline state as well as in aqueous solution, stabilized by electrostatic, polarization, and H-bonding interactions with the solvent.^{22–26} In the gas phase, where these intermolecular interactions have no effect, amino acids exist in their nonionized forms.^{22,23} Zwitterion formation in aqueous solution occurs by means of the ionization of the carboxylic acid and amino groups. These two charged groups, COO^- and NH_3^+ , strongly interact with each other and with the aqueous environment. There are a number of theoretical studies on the alanine zwitterion (ALAZW) using in vacuo calculations, with or without applying reaction fields, mainly for analysis of the vibrational spectra obtained for the solid phase and/or aqueous solution form of the ALAZW and its deuterated isotopologues.^{20,21}

The vibrational frequency assignment for the ALAZW and its deuterated isotopologues in aqueous solution has previously been reported by Diem and co-workers.^{27–30} These assignments are based primarily on aqueous solution-phase Raman spectra together with results of infrared (IR) and Raman solid-phase

[§] Permanent address: Department of Medicinal Chemistry, School of Pharmacy, Tehran University of Medical Sciences, P.O. Box 14155/6451, Tehran, Iran.

* Author to whom all correspondence should be addressed. Tel: +49 6221 42 2369. Fax: +49 6221 42 2333. E-mail: S.Suhai@DKFZ-Heidelberg.de.

spectra in conjunction with a Urey–Bradley normal coordinate analysis.²⁷ Ab initio calculations of the Raman and Raman optical activity (ROA) intensities of isolated ALAZW resulted in good agreement between the experimental and theoretical results at the restricted Hartree–Fock (RHF)/6-31G* level of theory in the lower frequency region.²⁰ However, the calculated ROA signs of several bands did not correspond to the experiment and the calculated frequency separation for the antisymmetric and symmetric amino deformations and antisymmetric and symmetric carboxylate stretches were reported to be much larger than the experimental values. To simulate solvent effects, Yu and co-workers²¹ performed RHF/6-31G* Onsager self-consistent reaction-field geometry optimization and force constant calculations for the ALAZW and found better agreement between the calculated ROA signs and intensities and the experimental values.

In the present work, we studied the effect of the presence of explicit water molecules on the calculated geometries and vibrational spectra of the ALAZW. The results of the geometry optimizations are totally different after the inclusion of explicit solvent molecules in the calculations. The predicted structure of the ALAZW in the presence of explicit water molecules is completely different from the previously reported structures for this molecule.

Recently it has been shown that B3LYP optimized geometries, Hessians, and atomic polar tensors (APT) combined with RHF distributed origin gauge atomic axial tensors (AAT) calculated with split valence or larger basis sets are able to predict accurately the vibrational absorption (VA) and vibrational circular dichroism (VCD) spectra of simple and medium sized organic molecules.^{31–38} Other groups had previously shown that DFT level vibrational absorption calculations are more accurate than RHF level calculations.^{39,40} Finally, DFT methods have been used to analyze the vibrational spectra of models for lipids⁴¹ and nucleic acids.^{42,43} Most of the previous work has been done on systems where there was only one possible structure and the problem of multiple minima was not addressed. Also most of the work has been done on systems where the spectra did not change significantly when the solvent was changed. This work is also an attempt to extend and document the methodology of density functional theory (DFT) as applied to the calculation of the VA, VCD, and Raman spectra of simple biological molecules where (i) there are several low energy structures and (ii) the effect of the solvent is a large one. These two problems should be addressed if VA, VCD, and Raman spectra are to be routinely applied to answer structural questions in molecular biology and biophysics. L-Alanine is a very good molecule to test the applicability of using these three types of spectroscopy to answer the simple question: what is (are) the structure(s) of this simple molecule in aqueous solution. One may assume that such a simple molecule has only a single low energy structure, and indeed, many workers who have studied this molecule have assumed this fact.

Here we would like to document that including the explicit water molecules in the optimization of the ALAZW structure(s), one comes to a very different conclusion about the predicted structure of the ALAZW. The calculated vibrational properties of this small amino acid can be significantly influenced by very small rearrangements in the relative position of the neighboring water molecules in the first hydration shell. These points should be considered while attempting to use the theoretically derived structures to interpret the experimental results which are applied to answer the question of the ALAZW structure in solution.

Methods

Initial Geometries. The ALAZW was constructed using the amino acid library of the builder module of the program InsightII.⁴⁴ After assignment of the charges and potential types, the structure was minimized using the cff91 force field of the program. The optimized structure was then hydrated using a preequilibrated water box of the size of $15 \times 15 \times 15 \text{ \AA}$ which was large enough to cover at least 5 \AA around the ALAZW. The whole assembly was then considered for a molecular dynamic (MD) simulation applying periodic boundary conditions. The MD simulation was performed for 1 ps at 300 K, using dielectric constant of 1 and a nonbonded cutoff radius of 20 \AA . Examination of the trajectory of the MD simulation showed that in order to involve the two hydrophilic groups of the ALAZW, namely the COO^- and NH_3^+ groups, in the first hydration shell, at least four water molecules were needed. For this reason we extracted the complex structure of the ALAZW and the four closest water molecules out of the hydration box and set up a second MD in order to examine the possible arrangements of this complex (ALAZW and four waters).

In the next step the optimized structure of the ALAZW and of its neighboring four water molecules was used as the starting geometry for a 10 ps MD simulation at 300 K, using again the dielectric constant of 1. In order to have a complete sampling, we extracted the 200 lowest potential energy snapshots out of the generated MD trajectory and minimized them. Superimposition of the minimized structures reveals that the whole data set converges to a cluster of 16 conformers. Application of a semiempirical optimization at the PM3 level of theory decreases the number of different arrangements to five structures which were used in further ab initio calculations. PM3 semiempirical calculations were performed by the MOPAC 93 program.

Ab Initio Calculation. B3LYP/6-31G* level calculations were performed with GAUSSIAN 94⁴⁵ on an IBM SP2 computer. During the application of the Onsager continuum model, the recommended cavity radius of the volume calculation of solute structure and the dielectric constant of 80.0 were used.

The VA, VCD, and Raman spectra of the ALAZW structures have been calculated using the B3LYP/6-31G* Hessian and APT, RHF/6-31G** APT, distributed origin gauge AAT, and RHF/6-311+G** electric dipole–dipole polarizability derivatives. B3LYP/6-31G* level analytical Hessian (second derivatives of the energy with respect to nuclear displacements) and APT (first derivative of the electric dipole moment with respect to nuclear displacement) calculations have been implemented in GAUSSIAN 94⁴⁶ and CADPAC.^{47,48} The analytical implementation of the distributed origin gauge AAT, APT, electric dipole–dipole polarizability derivatives, and Hessians at the RHF level has been performed using CADPAC. The calculation of VA and VCD spectra requires the calculation of the APT and AAT along with the Hessian. We have calculated the distributed origin gauge AAT at the RHF/6-31G** level with CADPAC and the Hessian and APT at the B3LYP/6-31G* level with GAUSSIAN 94. The equations for the VA and VCD calculations are the same as those used in our previous work on *N*-acetyl-L-alanine *N'*-methylamide³⁶ so we do not give them here.

The calculation of the Raman scattering intensities requires the calculation of the polarizability derivatives $\alpha_{ij}^{\lambda\alpha}$:

$$\alpha_{ij}^{\lambda\alpha} = \left(\frac{\partial^3}{\partial X_{\lambda\alpha} \partial E_i \partial E_j} W_G(\vec{R}, E_i, E_j) \right)_{\vec{R}_e, E_i=0, E_j=0} = \left(\frac{\partial}{\partial X_{\lambda\alpha}} \alpha_{i,j}(\vec{R}) \right)_{R_e} \quad (1)$$

where W_G is the ground state potential energy surface in the presence of two static electric fields, E_i and E_j , and $X_{\lambda\alpha}$ is the nuclear displacement of atom λ along the Cartesian coordinate, $\alpha = x, y, z$.

CADPAC has implemented the analytical calculation of polarizability derivatives at the RHF level^{47,48} as has GAUSSIAN, Inc.,⁴⁶ but neither to date has at the DFT level of theory. Recently, Johnson and Florian⁴⁹ have implemented the polarizability derivatives at the DFT level of theory using the finite-field numerical second differentiation of analytically calculated energy derivatives. This is the same method as used by Komornicki and McIver to calculate Raman intensities by Hartree–Fock theory in their program GRADSCF.⁵⁰ After the polarizability derivatives have been calculated, they can be combined with the vibrational frequencies and normal mode vectors to predict the differential Raman scattering cross sections, scattering activities and depolarization ratios. The absolute differential Raman scattering cross section is given by

$$\left(\frac{d\sigma_j}{d\Omega}\right) = \frac{2^4\pi^4}{45} \frac{(\nu_0 - \nu_j)^4}{1 - \exp\left[-\frac{h\nu_j}{kT}\right]} \frac{h}{8\pi^2c\nu_j} S_j \quad (2)$$

where ν_0 is the incident laser frequency and $(\nu_0 - \nu_j)$ is the scattered frequency, h , c , and k are Planck's constant, the speed of light and Boltzmann's constant, respectively. S_j is the Raman scattering activity, given by

$$S_j = g_j(45\bar{\alpha}_j^2 + 7\bar{\beta}_j^2) \quad (3)$$

where g_j is here the degeneracy of the j th transition of energy $h\nu_j$ and $\bar{\alpha}_j^2$ and $\bar{\beta}_j^2$ are given by

$$\bar{\alpha}_j^2 = \frac{1}{9}(S_{\lambda\alpha,j}\alpha_{xx}^{\lambda\alpha} + S_{\lambda\alpha,j}\alpha_{yy}^{\lambda\alpha} + S_{\lambda\alpha,j}\alpha_{zz}^{\lambda\alpha})^2 \quad (4)$$

$$\begin{aligned} \bar{\beta}_j^2 = \frac{1}{2}\{ & (S_{\lambda\alpha,j}\alpha_{xx}^{\lambda\alpha} - S_{\lambda\alpha,j}\alpha_{yy}^{\lambda\alpha})^2 + \\ & (S_{\lambda\alpha,j}\alpha_{xx}^{\lambda\alpha} - S_{\lambda\alpha,j}\alpha_{zz}^{\lambda\alpha})^2 + (S_{\lambda\alpha,j}\alpha_{yy}^{\lambda\alpha} - S_{\lambda\alpha,j}\alpha_{zz}^{\lambda\alpha})^2 + \\ & 6[(S_{\lambda\alpha,j}\alpha_{xy}^{\lambda\alpha})^2 + (S_{\lambda\alpha,j}\alpha_{yz}^{\lambda\alpha})^2 + (S_{\lambda\alpha,j}\alpha_{xz}^{\lambda\alpha})^2]\} \end{aligned} \quad (5)$$

where the matrix $S_{\lambda\alpha,j}$ interrelates normal coordinates Q_j to Cartesian displacement coordinates $X_{\lambda\alpha}$:

$$X_{\lambda\alpha} = \sum_j S_{\lambda\alpha,j} Q_j \quad (6)$$

We can make the expressions for the derivatives with respect to the normal coordinates more compact by noting that $\alpha_{\beta\gamma}^j = \alpha_{\beta\gamma}^{\lambda\alpha} S_{\lambda\alpha,j}$

$$\bar{\alpha}_j^2 = \frac{1}{9}(\alpha_{xx}^j + \alpha_{yy}^j + \alpha_{zz}^j)^2 \quad (4')$$

$$\begin{aligned} \bar{\beta}_j^2 = \frac{1}{2}\{ & (\alpha_{xx}^j - \alpha_{yy}^j)^2 + (\alpha_{xx}^j - \alpha_{zz}^j)^2 + (\alpha_{yy}^j - \alpha_{zz}^j)^2 + \\ & 6[(\alpha_{xy}^j)^2 + (\alpha_{yz}^j)^2 + (\alpha_{xz}^j)^2]\} \end{aligned} \quad (5')$$

The VA, VCD, and Raman spectra are simulated using Lorentzian line shapes. The full width at half the maximum was assumed to be 5 cm^{-1} for the mid-IR region (200–1800

cm^{-1}) and 10 cm^{-1} for the high frequency region (2800–3400 cm^{-1}) for the normal modes in spectra.

Results and Discussion

Geometries and Energies. Regarding the free rotation of different dihedral angles in the nonionized species of the L-alanine molecule, several reasonable conformers have been predicted for the amino acid.¹⁷ Because COOH and NH₂ groups of nonionized species ionize to two symmetrical groups in the ALAZW (COO⁻ and NH₃⁺, respectively), a smaller conformational space is expected for the latter form. However, the strong electrostatic and/or H-bond interaction of these spatially close charged groups with each other should be kept in mind. Considering the well-known trend of H-bond formation between the oxygen atoms in the CO₂⁻ group and the hydrogens in the NH₃⁺ group, a strong interaction between the carboxylate and ammonium groups of the ALAZW is expected. With this regard, four different arrangements can be intuitively imagined for the ALAZW monomer in the absence of solvent molecules. These possible structures are schematically depicted in Figure 2 and were used as the starting geometries for further optimizations using different methodological approaches. The assigned names in Figure 2 reflect the atoms which are involved in the intramolecular interaction of two charged groups in the conformer. For example, HHO means that in this conformer one of the oxygen atoms of the carboxylate group is facing and interacting with two hydrogen atoms of the ammonium group. The four different conformers are constructed by different combinations of two torsion angles, HNC_αC' (0° or 60°) and OC'C_αN (0° or 90°). These angles are of great importance in the determination of the backbone structure of the polypeptide molecules.

In the first set of calculations, we started from all of the starting geometries shown in Figure 2 and optimized them with different force fields, including empirical, semiempirical, or ab initio calculations. The results of the first set of calculations showed that depending on the nature of the applied method, different final structures could be obtained after full geometry optimizations. All of the molecular mechanics force fields ended up with a slightly rotated HHOO structure (Figure 2). The results of the semiempirical calculations were not as unique as the results of molecular mechanics force fields, and the shape of the final structure was dependent on both the starting conformation and the method applied (MNDO, AM1, or PM3). In the case of ab initio calculations, all RHF optimizations of the ALAZW resulted in the HO structure. This result was independent of the size and the polarization extent of the basis set (6-31G*, 6-31G**, 6-311+G*). The application of the Onsager dipole continuum model using different cavity sizes (recommended radius or recommended radius minus 0.5 Å) and different dielectric constants (4.0, 40.0 or 80.0) had no effect on this conclusion. Other internal coordinates of the ALAZW, such as bond lengths and bond angles, however, were influenced by inclusion of the continuum model in the calculation. The HO conformer is the structure reported in all of the previous theoretical ab initio studies on the ALAZW structure.^{20,21}

There are a number of studies demonstrating problems with RHF level theoretical calculations on amino acids, including, most importantly, the inability of the RHF level of theory to predict the relative energies of the N–H···O and O–H···N H-bonded conformers in these systems. Therefore, we repeated the calculations at B3LYP DFT and MP2 levels of theory. Application of the B3LYP DFT method resulted in a completely different picture. On the B3LYP potential energy surface there

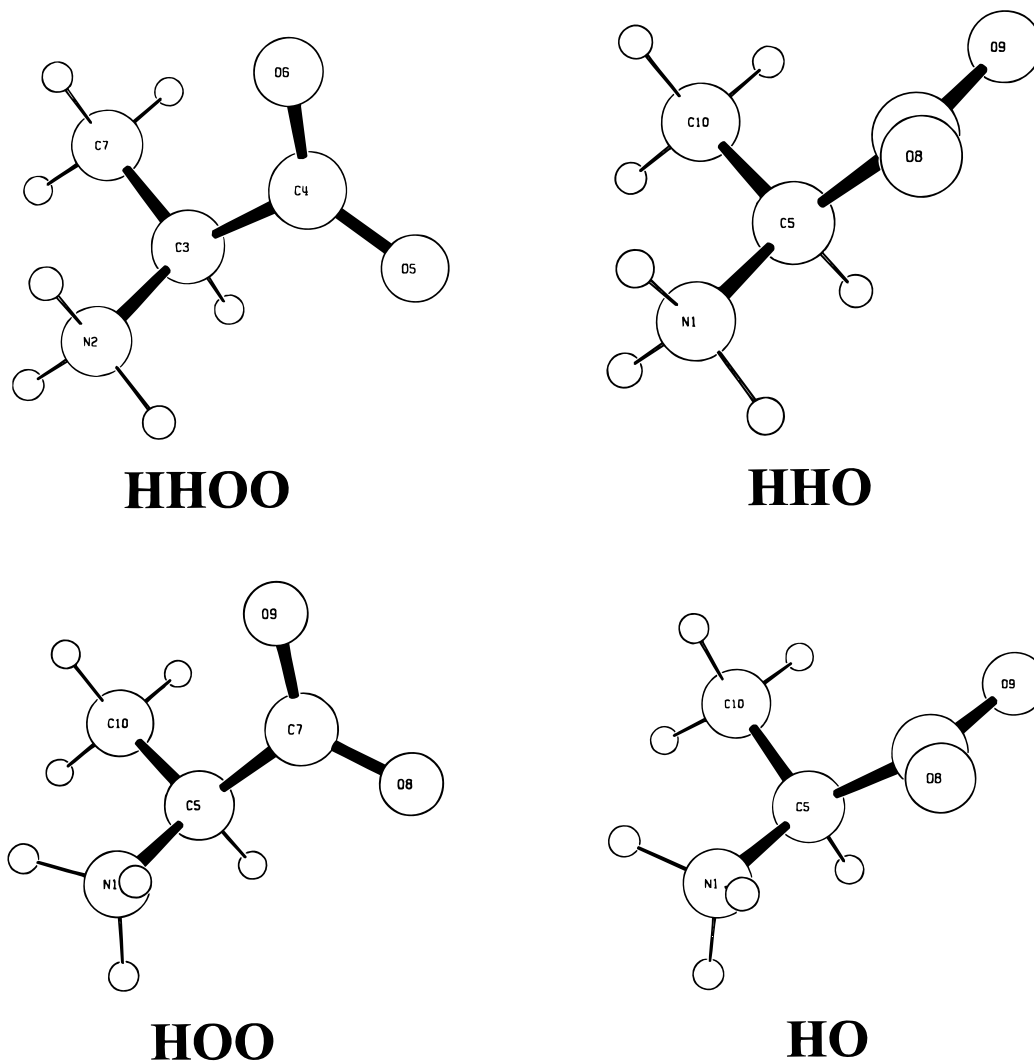


Figure 2. Different conformers of the ALAZW which were used as the starting structures in the geometry optimization and hydration procedures described in the methods section. The labels reflect the atoms which are involved in the intramolecular interaction of carboxylate and ammonium groups in the ALAZW.

is no barrier to conversion of the ALAZW to the nonionized species. In our calculations, independent of the size and the level of polarization of the basis set, we were not able to locate a stable ALAZW on the B3LYP/6-31G* potential energy surface. In the case of all starting geometries (Figure 2), after approaching the transient HO conformer, a proton transfer occurred and the ALAZW converted to the nonionized species. The results from MP2 calculations were similar to the B3LYP results. The ALAZW molecule is not stable at MP2 level and will be converted to the neutral species after the transfer of a proton from NH_3^+ group to the CO_2^- group. The instability of the zwitterion structure within gas phase calculations has been previously reported for glycine in a detailed ab initio electronic structure investigation.^{51,52} It has been concluded that there is no minimum on the gas phase potential energy surface corresponding to the glycine zwitterion and with basis sets which contain polarization functions on hydrogen atoms (e.g., 6-31G**), the intramolecularly hydrogen-bonded zwitterion species of glycine collapses to the nonionized species at both independent particle and electron correlated levels. Because of these observations, we decided to study the effect of the inclusion of explicit solvent molecules on the calculated stability of ALAZW and on the conformational preference of the molecular system.

In order to find the optimum number and position of water molecules to be explicitly included in the ab initio calculations,

we started with empirical MD simulations using periodic boundary conditions for the ALAZW hydrated in a box of water molecules, as described in the methods section. Examination of the trajectories of the MD simulations showed that, although the solute structure was quite flexible and could freely rotate around the $\text{C}_\alpha\text{-N}$ and $\text{C}_\alpha\text{-C}'$ bonds, in most parts of the simulations, the ALAZW adopted conformers were very close to the HHOO structure. Furthermore, it was also found that, in order to hydrate both the NH_3^+ and COO^- groups in the ALAZW, at least four water molecules were needed. Consequently, for the next step of the study the ALAZW was hydrated with four explicit water molecules.

To sample possible relative positions of the solvent molecules, the next MD simulation was performed on the complex of the ALAZW and four water molecules, as described in the methods section. After a PM3 semiempirical geometry optimization, the whole data set of 200 snapshots of MD trajectory, which were selected on the basis of their relatively low potential energy, converged to one of five conformers. In all of these structures the ALAZW can be best described as a slightly rotated HHOO conformer. These conformers were used for the further ab initio calculations.

In the presence of explicit water molecules all of the conformers retained their starting HHOO configuration during the ab initio optimization. From now on we call these five

TABLE 1: B3LYP/6-31G* Bond Lengths, Bond Angles, and Torsional Angles for the Six ALAZW Conformers^a

	A ^b	A' ^c	B	B'	C	C'	D	D'	E	E'	F	F'
R(N2-H1)	1.049	1.044	1.056	1.051	1.053	1.050	1.055	1.052	1.040	1.038	1.047	1.045
R(C3-N2)	1.519	1.516	1.519	1.518	1.514	1.510	1.517	1.517	1.515	1.514	1.512	1.506
R(C4-C3)	1.571	1.571	1.567	1.566	1.567	1.566	1.564	1.562	1.575	1.572	1.564	1.562
R(O5-C4)	1.264	1.260	1.276	1.278	1.257	1.256	1.241	1.244	1.255	1.259	1.289	1.281
R(O6-C4)	1.250	1.258	1.242	1.243	1.255	1.260	1.276	1.280	1.255	1.257	1.230	1.246
R(C7-C3)	1.521	1.522	1.520	1.521	1.525	1.526	1.523	1.524	1.522	1.523	1.527	1.530
R(H8-C3)	1.093	1.093	1.094	1.094	1.092	1.091	1.092	1.092	1.095	1.093	1.095	1.095
R(H9-C7)	1.093	1.093	1.093	1.093	1.093	1.094	1.094	1.094	1.093	1.092	1.096	1.096
R(H10-C7)	1.094	1.095	1.094	1.094	1.094	1.095	1.095	1.095	1.093	1.095	1.092	1.092
R(H11-C7)	1.096	1.095	1.096	1.095	1.097	1.096	1.097	1.095	1.097	1.095	1.097	1.095
R(H12-N2)	1.036	1.037	1.055	1.054	1.036	1.035	1.056	1.050	1.052	1.048	1.048	1.044
R(H13-N2)	1.047	1.054	1.034	1.038	1.037	1.045	1.033	1.039	1.034	1.043	1.034	1.046
A(C3-N2-H12)	107.5	107.8	109.3	109.6	108.6	109.4	108.4	108.4	109.1	108.0	109.8	109.7
A(C3-N2-H13)	109.5	109.6	112.0	111.5	110.4	109.3	111.4	111.2	112.6	111.9	110.6	111.8
D(C4C3N2H1)	62.1	61.2	49.1	50.6	64.5	61.0	64.3	64.2	48.2	58.9	59.2	60.1
D(O5C4C3N2)	86.7	83.9	73.0	72.1	116.6	118.8	103.0	105.5	60.6	89.0	-0.5	-2.8
D(H9C7C3H8)	178.4	178.9	-177.9	-178.7	178.7	178.1	-177.4	-178.7	177.3	-177.9	177.2	177.7

^a In angstroms and degrees. ^b A, B, C, D, E, and F refer to the ALAZW plus four water molecules. ^c A', B', C', D', E', and F' refer to the ALAZW plus four water molecules optimized using the Onsager model.

different structures of the ALAZW and four water molecules A, B, C, D, and E (from the most stable conformer to the less stable one, respectively). On the basis of these theoretical results, in the presence of explicit water molecules, the HHOO structure is a stable conformer of the ALAZW. This conformer of the ALAZW can not be located during the in vacuo calculations or even by application of reaction field solvent models in the absence of explicitly included solvent molecules. Previously Barron and co-workers²⁰ and Yu and co-workers²¹ were able to get stable zwitterionic structures for L-alanine utilizing RHF/6-31G* isolated molecule calculations and within the RHF/6-31G* Onsager continuum model, respectively. The calculations did not include any electron correlation and the structure was different than the global minimum we found by the inclusion of explicit waters. We may conclude, therefore, that inclusion of explicit water molecules seems to be very important to get this structure, which may exist and be the most prominent species in aqueous solution.

Because of the molecular mechanics nature of the MD simulations, which were used for generating the starting complex structures, and because of the preference of the HHOO conformer in the applied molecular mechanics force field, we could have missed other possible conformers which may also be stable in the presence of explicit solvent molecules within ab initio calculations. Therefore, we decided to check for the existence of other stable ALAZW conformers in the presence of four water molecules. To this end, three other starting conformers in Figure 2, the HO, HHO, and HOO labeled structures, were hydrated by adding four water molecules to them. The complexes were then optimized using the same ab initio approach. Very interestingly, after geometry optimization both HO (the only stable geometry in the gas phase ab initio RHF calculations) and HOO structures converted to the HHOO conformer in the presence of the four water molecules. The HHO conformer, however, was stable during the geometry optimization in the presence of the four water molecules. We have included this complex as the sixth conformer (conformer F) into the further analysis.

B3LYP/6-31G* optimized geometries of the six ALAZW conformers and their neighboring water molecules are depicted in Figure 3. The bond lengths, valence angles, and torsion angles of the ALAZW for these conformers are presented in Table 1. As one can see, the largest and most obvious difference in the solute structure is the difference in the two C-O bond lengths. They vary by as little as 0.0005 Å in one conformer

(conformer E) and by as much as 0.0594 Å in another one (conformer F). There are clearly very large structural differences between the various conformers. The second most obvious observation is the difference between the N-H bond lengths which is a function of the H-bonding between the hydrogen atoms of the ammonium group and the oxygen atoms of the carboxylate group or to oxygen atoms of neighboring water molecules. The HNC_αC_β and OCC_αC_β torsion angles are also strongly coupled to the NC_αC' valence angle which varies by 6.5°, a very large variation in a simple valence angle.

The relative energies of the A-F structures are given in Table 2. The first four conformers (A-D) are separated by less than 1.0 kcal/mol. By including the zero point energy corrections to the total energies, we find that the global minimum is now 0.6 kcal/mol lower than the next highest energy conformer. Since our zero point energy corrections include, however, water modes, the energies which are not corrected may be more useful. In any case, it seems possible that a conformational equilibrium may exist between the low energy conformers.

Considering the relative positions of the surrounding water molecules, comparison of the geometries depicted in Figure 3 shows that, in the case of conformers A-E, where the ALAZW adopts HHOO structure, the arrangement of the neighboring water molecules relative to the ALAZW can also be considered as a significant difference between the conformers. Therefore, the differences in calculated relative energies can be, at least partly, related to the differences in the number and way of the hydrogen bonds between the ALAZW and solvent molecules. Conformer F demonstrates, both structurally and energetically, a completely different behavior. It can easily be understood that there is a strong coupling between the arrangement of the surrounding water molecules and the internal properties of the solute. Since the arrangement of water molecules in the first solvating shell may be significantly influenced by the presence of the second hydration shell, consideration of the calculated relative energies for further conclusions should be carefully done.

In order to study the possible influence of inclusion of further solvation effects into the calculation on the obtained energies, all obtained complex structures of the ALAZW and of the four water molecules were reoptimized using the same basis set and level of theory, but with the implicit inclusion of the solvent effects as the Onsager continuum model. The recommended cavity radius obtained from the volume calculation of the solute and dielectric constant of 80.0 were used in this set of calculations.

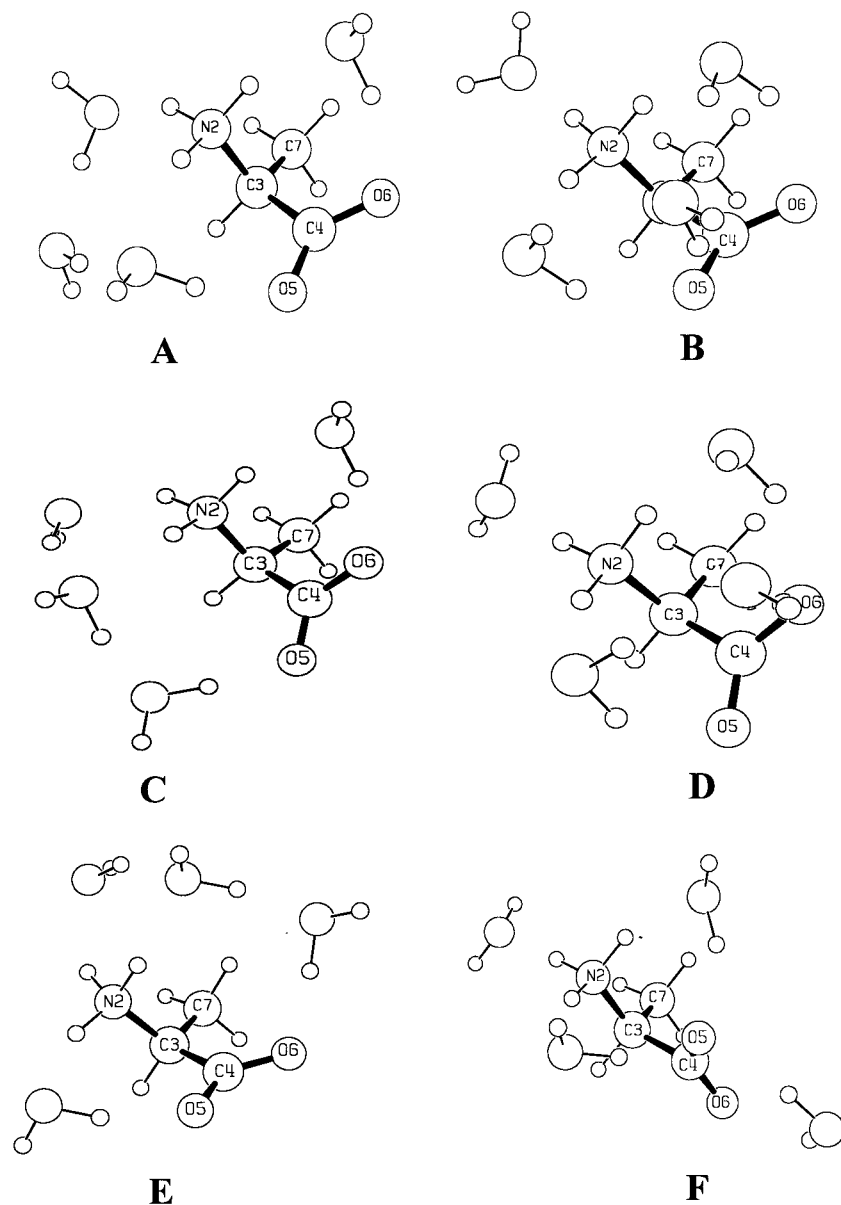


Figure 3. B3LYP/6-31G* optimized geometries of six different ALAZW conformers and their neighboring water molecules. In all structures each hydrogen atom of the ammonium group and oxygen atom of the carboxylate group is involved in at least one hydrogen bond with the water molecules.

TABLE 2: Molecular Total Energies (hartree) and Relative Energies (kcal/mol) for Six Different Conformers of the ALAZW and Four Water Molecule Assembly

conformer ^a	B3LYP/6-31G*	RE ^c	REC ^d	conformer ^b	B3LYP 6-31G*	RE	REC
A	-629.457875	0.000	0.000	A'	-629.465338	3.711	4.676
B	-629.457657	0.137	0.619	B'	-629.463596	4.804	5.939
C	-629.456801	0.674	0.634	C'	-629.464675	4.127	4.863
D	-629.456418	0.915	1.246	D'	-629.464847	4.020	4.965
E	-629.454257	2.270	2.059	E'	-629.460358	6.836	7.437
F	-629.440439	10.941	9.450	F'	-629.471251	0.000	0.000

^a ALAZW with four water molecules. ^b ALAZW with four water molecules plus the Onsager model. ^c RE: relative energy in kcal/mol (relative to the lowest energy conformer). ^d REC: relative energy corrected including zero point energy.

In Table 2 we also present the relative energies of the six conformers (**A'**–**F'**), which have been optimized by adding the Onsager continuum model to the ALAZW and four water complexes. The point here was to see what the effect of the continuum model would be on the relative energies and structures of the six conformers as well as the movement of the water molecules from their initial positions. As one can see from Table 2 the relative energies have substantially

changed. The relative energies of the conformers, particularly in the case of the **F'** structure, have been strongly influenced by the presence of the reaction field. The conformer **F**, which is the less stable structure in gas phase calculations without applying the continuum model (Table 2), is now the energetically most favored structure (**F'**) among the calculated conformers. Clearly the Onsager model has greatly changed the picture. However, because the relative energies vary so much between

the two models, we do not think that we can determine which structure(s) is (are) present in aqueous solution from the energies alone. With such a large change in the relative energies we now look at the structural differences which could account for these effects on the relative energies and spectroscopic differences which could be used to distinguish the structures from each other.

The optimized geometries of this set of calculations including the Onsager continuum model are referred to as **A'**–**F'** structures and are also reported in Table 1. It can clearly be seen that, except for the N–H and C–O bond lengths which can be directly influenced by the water molecules hydrogen bonded to them, after the inclusion of the continuum model the geometries of the solute do not change significantly. The HHOO conformer is still a stable conformer after implicitly including further solvation effects. The C–O bond lengths vary with torsion angle about the C_{α} –C' bond, but not as much as without the Onsager model. The $NC_{\alpha}C'$ valence angle still varies by over 6.0° .

In order to study the effect of the solvation effects by explicitly including water molecules and application of a continuum model on the relative stabilities of neutral and zwitterionic forms of L-alanine, we have also optimized the neutral species of the solute in the presence of four water molecules with and without application of the Onsager model reaction field. Two different and independent approaches were used in order to get the starting geometries for neutral species of L-alanine and four water molecules. In the first approach (I) we started with the most energetically favorable conformer of neutral form of alanine, as reported by a recent ab initio study,¹⁹ and added four water molecules to it (conformer I). In the second approach (II) we started from the most stable cluster of ALAZW and four water molecules (conformer A) in the present study. We converted the ALAZW to the neutral species (conformer II) by forcing a proton to be transferred from NH_3^+ group to the CO_2^- group by gradually increasing the corresponding N–H bond distance. The hydrogen bonds of NH_3^+ and CO_2^- groups to one of the water molecules facilitate the proton transfer and the proton transfers via this water molecule. We would like to compare the energies of these clusters of neutral alanine and four water molecules with the corresponding clusters of ALAZW and four water molecules. With this respect, the second approach may result in a more homogeneous cluster which can be used in comparison of the energies of neutral alanine and ALAZW hydrated with four water molecules. The structures were then fully optimized using the B3LYP/6-31G* level of theory. The molecular total energies calculated for the fully optimized alanine neutral species and four water molecules obtained from these two approaches are -629.445417 and -629.453576 hartree, respectively. Compared to the molecular total energy of the conformer A (ALAZW and four water molecules), -629.457875 hartree, these clusters are less stable 7.82 and 2.70 kcal/mol, respectively. The optimized structure of the second approach which is energetically more stable was used as the starting structure for the Onsager model optimization of the system. After the inclusion of the reaction field into the calculation, the molecular total energy of the fully optimized structure of conformer II is calculated to be -629.455937 hartree. As compared to the corresponding molecular total energy of the ALAZW and four water molecules optimized using Onsager model, -629.465338 hartree, conformer II is 5.90 kcal/mol less stable. Regarding these observations, it seems that inclusion of explicit water molecules into the calculations not only creates a barrier against

the proton transfer which happens in DFT and MP2 optimization of the ALAZW but also influences the shape of the potential energy surface with respect to the relative energies of the neutral and zwitterionic species. We have found the zwitterionic structure more stable than the neutral species, so we are able to reproduce this experimentally observed effect. However, it should be kept in mind that we have studied only two of the possible structures of the neutral species and four water molecules. It is possible that one can find more energetically favorable clusters by having a more systematic approach.

Vibrational Absorption. One of the most relevant experimental approaches toward the structure elucidation of chemical compounds is vibrational spectroscopy. The calculation of the Raman spectra of biological molecules in the presence of water is now feasible. The calculations for simple models provide benchmark results for the calculation of Raman spectra of larger biological molecules in aqueous solution. Because of the complexity of the spectra obtained, many investigators use theoretical calculations to assist the interpretation of the experimental results.^{20,21,31–43} Recently B3LYP level analytical Hessian calculations have been implemented in GAUSSIAN 94⁴⁶ and CADPAC.^{47,48} These force fields have been shown to be more accurate than RHF level Hessians which must be scaled to get good agreement with both experimental frequencies and IR absorption, VCD, and Raman intensities. The nature of the normal modes have been shown to depend very much on the scaling scheme one chooses to scale the Hessian. The advantage of the B3LYP level of theory is that the Hessians appear to be accurate enough to predict the IR absorption and VCD and Raman intensities when coupled with accurate APT, distributed origin gauge AAT, and electric dipole–dipole polarizability derivatives without scaling. The number of molecules for which the B3LYP Hessians have been calculated and then using the resulting APT and RHF distributed origin gauge AAT the IR absorption and VCD spectra have been predicted has been quite limited.^{31–43} The good agreement shown until now was limited to a small number of functional groups and the comparison has been with measurements of the VA and VCD spectra of molecules in nonpolar solvents. We would like to extend here that work to include the ALAZW structure found in aqueous solution since the ALAZW is not stable in the gas-phase according to our ab initio B3LYP/6-31G* calculations, and we have to explicitly include water molecules to stabilize this structure. In this section we present the calculated VA spectra of the structures **A'**–**F'** (ALAZW and four water molecules optimized using Onsager model) in order to see the effect of the inclusion of explicit water molecules on the predicted spectra of the system. In order to further study the predicted structures, vibrational analysis of all conformers was performed as described in the methods section. The vibrational internal coordinates of ALAZW which are used in the analysis of the normal modes are presented in Table 3. These local symmetry vibrational coordinates are linear combinations of the simple valence coordinates and are recommended by Pulay⁵³ when scaling quantum mechanical force fields. These coordinates are also useful in assigning the calculated frequencies to the normal modes, which are more convenient in spectroscopic analyses.

In Table S1 (Supporting Information) we align the calculated vibrational frequencies with those measured by Diem and co-workers.^{27–30} The results are presented for the six conformers of the ALAZW stabilized by four water molecules and Onsager continuum model along with our vibrational assignment obtained on the basis of potential energy distribution analysis. The

TABLE 3: Internal Coordinate Definition for L-Alanine Zwitterion Monomer^a

no	mode	nature	no	mode	nature
q ₁	R ₁	N-H stretch	q ₁₈	$(\alpha'_1 + \alpha'_2 + \alpha'_3 - \beta'_1 - \beta'_2 - \beta'_3)/\sqrt{6}$	CH ₃ sym. deformation
q ₂	R ₂	N-H stretch	q ₁₉	$(2\alpha'_1 - \alpha'_2 - \alpha'_3)/\sqrt{6}$	CH ₃ asym. deformation
q ₃	R ₃	N-H stretch	q ₂₀	$(\alpha'_2 - \alpha'_3)/\sqrt{2}$	CH ₃ asym. deformation
q ₄	R ₄	C _β -H stretch	q ₂₁	$(2\beta'_1 - \beta'_2 - \beta'_3)/\sqrt{6}$	CH ₃ rocking
q ₅	R ₅	C _β -H stretch	q ₂₂	$(\beta'_2 - \beta'_3)/\sqrt{2}$	CH ₃ rocking
q ₆	R ₆	C _β -H stretch	q ₂₃	$(2\beta''_1 - \beta''_2 - \beta''_3)/\sqrt{6}$	C _α -H rocking
q ₇	R ₇	C _α -H stretch	q ₂₄	$(\beta''_2 - \beta''_3)/\sqrt{2}$	C _α -H rocking
q ₈	R ₈	C'-O stretch	q ₂₅	$(4\alpha_{XCX} + \alpha_{XCZ} + \alpha_{YCZ})/\sqrt{18}$	XCY deformation
q ₉	R ₉	C'-O stretch	q ₂₆	$(4\alpha_{XCZ} + \alpha_{XCX} + \alpha_{YCZ})/\sqrt{18}$	XCY deformation
q ₁₀	R ₁₀	N-C _α stretch	q ₂₇	$(4\alpha_{YCZ} + \alpha_{XCX} + \alpha_{XCZ})/\sqrt{18}$	YCZ deformation
q ₁₁	R ₁₁	C _α -C' stretch	q ₂₈	$(2\alpha''' - \beta'''_1 - \beta'''_2)/\sqrt{6}$	CO ₂ sym. deformation
q ₁₂	R ₁₂	C _α -C _β stretch	q ₂₉	$(\beta'''_1 - \beta'''_2)/\sqrt{2}$	CO ₂ rocking
q ₁₃	$(\alpha_1 + \alpha_2 + \alpha_3 - \beta_1 - \beta_2 - \beta_3)/\sqrt{6}$	NH ₃ sym. deformation ^b	q ₃₀	oop	CO ₂ out of plane wagging
q ₁₄	$(2\alpha_1 - \alpha_2 - \alpha_3)/\sqrt{6}$	NH ₃ asym. deformation	q ₃₁	τ ₁	N-C _α torsion
q ₁₅	$(\alpha_2 - \alpha_3)/\sqrt{2}$	NH ₃ asym. deformation	q ₃₂	τ ₂	C'-C _α torsion
q ₁₆	$(2\beta_1 - \beta_2 - \beta_3)/\sqrt{6}$	NH ₃ rocking	q ₃₃	τ ₃	C _β -C _α torsion
q ₁₇	$(\beta_2 - \beta_3)/\sqrt{2}$	NH ₃ rocking			

^a R₁ = H₁-N₂, R₂ = H₁₂-N₂, R₃ = H₁₃-N₂, R₄ = H₉-C₇, R₅ = H₁₀-C₇, R₆ = H₁₁-C₇, R₇ = H₈-C₃, R₈ = O₆ = C₄, R₉ = O₅ = C₄, R₁₀ = N₂-C₃, R₁₁ = C₃-C₄, R₁₂ = C₃-C₇, α₁ = H₁-N₂-H₁₃, α₂ = H₁-N₂-H₁₂, α₃ = H₁₂-N₂-H₁₃, β₁ = H₁₂-N₂-C₃, β₂ = H₁₃-N₂-C₃, β₃ = H₁-N₂-C₃, α'₁ = H₉-C₇-H₁₀, α'₂ = H₉-C₇-H₁₁, α'₃ = H₁₀-C₇-H₁₁, β'₁ = H₁₁-C₇-C₃, β'₂ = H₁₀-C₇-C₃, β'₃ = H₉-C₇-C₃, β''₁ = H₈-C₃-N₂, β''₂ = H₈-C₃-C₄, β''₃ = H₈-C₃-C₇, α_{XCX} = C₄-C₃-N₂, α_{XCZ} = C₄-C₃-C₇, α_{YCZ} = N₂-C₃-C₇, α'''₁ = O₅-C₄-O₆, β'''₁ = C₃-C₄-O₅, β'''₂ = C₃-C₄-O₆, oop = C₃-C₄-O₅-O₆, τ₁ = H₁-N₂-C₃-C₄, τ₂ = N₂-C₃-C₄-O₆, τ₃ = H₉-C₇-C₃-N₂. ^b sym. = symmetric. asym. = asymmetric.

calculated vibrational absorption spectra for the most energetically favorable conformer, conformer **F'**, are also presented in Table 4. The vibrational spectra to be discussed are also depicted schematically in Figure 4a and b. The frequencies and their corresponding absorption intensities have been calculated at the optimized geometry and using the B3LYP/6-31G* Hessians and APT.

As can be seen, the bond lengths and valence angles of the charged carboxylate and ammonium groups and, therefore, the vibrational modes which are dependent on these structural properties, can be significantly influenced by the presence of the neighboring hydrogen-bonded water molecules. Evaluation of the potential energy distributions of the hydrogen stretching modes (4000–2000 cm⁻¹) of the calculated spectra is quite helpful in assigning the stretching modes in this region (q₁ – q₇). As can be seen in Tables S1 and 4, the order of frequencies assigned to stretching of NH₃⁺, CH, and CH₃ groups is very different between the conformers. This can be related to the relatively large variations in the frequencies of stretching modes of the NH₃⁺ group which are due to bond length changes as a function of conformer. The calculated intense peaks related to NH₃⁺ stretching modes (q₁ – q₃) absorb at different frequencies in the different conformers. These findings are directly related to the different N–H bond lengths calculated for the different conformers which in turn may be due to the differences in the position of the H-bonded water molecules. As mentioned before, the calculated N–H bond length in the studied structures is one of the most variable parameters in our calculation (Table 1). This difference in bond lengths also appears for the three different N–H bonds within the same conformer. Assignment of the three NH₃⁺ stretching modes to two asymmetric and one symmetric modes in our calculations produces a splitting of 116, 231, 166, 188, and 80 wavenumbers in the asymmetric NH₃⁺ stretching modes for the first five conformers, respectively (Table S1). Generally only a very slight splitting is expected for the asymmetric stretching modes. However, it should be mentioned that this conclusion is made on the basis of the data obtained from the solid-state vibrational experiments of the ALAZW, where the positions of the water molecules around

TABLE 4: Vibrational Absorption, VCD, and Polarized Raman Spectra for Conformer F'

assn _{exp} ^a	ν _{exp} ^a	ν ^b	assignment	A _i ^c	A _i ^d	R _i ^e	R _i ^f	Å ⁴ / amu ^g
ν ^o NH ₃	3080	3164	q ₅ , q ₆	16	13	-11	-8	49
ν ^o NH ₃	3060	3142	q ₂ , q ₁	858	639	-4	-10	63
ν ^o NH ₃	3020	3137	q ₁ , q ₃	988	601	-71	-24	60
ν ^o CH ₃	3003	3135	q ₆ , q ₄	144	151	37	7	31
ν ^o CH ₃	2993	3113	q ₃ , q ₂ , q ₁ , q ₇	389	229	-30	-38	116
νC*H	2962	3093	q ₇	89	67	56	60	117
ν ^o CH ₃	2949	3064	q ₄ , q ₆ , q ₅	13	19	-2	-8	152
δ ^o NH ₃	1645	1759	q ₁₄ , q ₁₅	84	73	-17	-15	2
δ ^o NH ₃	1625	1750	q ₁₅ , q ₁₄	42	37	27	24	3
ν ^o CO ₂	1607	1695	q ₈ , q ₉	476	556	-53	-61	3
δ ^o NH ₃	1498	1635	q ₁₃	207	203	-9	-6	1
δ ^o CH ₃	1459	1536	q ₁₉ , q ₂₀	3	3	0	-2	5
ν ^o CH ₃	1459	1529	q ₂₀ , q ₁₉	13	11	-9	-14	7
δ ^o CO ₂	1410	1441	q ₁₈	66	53	68	59	1
δ ^o CH ₃	1375	1416	q ₂₃ , q ₁₈ , q ₁₇	8	12	48	56	3
δC*H	1351	1390	q ₉ , q ₁₁ , q ₁₆	110	125	-171	-168	5
δC*H	1301	1350	q ₂₄ , q ₉	141	142	38	48	2
ξNH ₃	1220	1290	q ₁₆ , q ₂₂ , q ₂₃ , q ₂₄	38	37	50	50	1
ξNH ₃	1145	1213	q ₁₇ , q ₂₄ , q ₂₃	61	57	1	-16	2
ν ^o CCN	1110	1133	q ₂₁ , q ₁₀ , q ₁₂	27	21	-11	-2	2
νCC(O ₂)	1001	1062	q ₂₂ , q ₁₆ , q ₁₂	12	10	3	2	2
ξCH ₃	995	1028	q ₁₂ , q ₂₁ , q ₁₀	5	10	-2	0	4
ξCH ₃	922	918	q ₁₀ , q ₁₁ , q ₂₂	13	10	-22	-18	3
ν ^o CCN	850	840	q ₂₈ , q ₁₀ , q ₁₁	42	49	20	15	9
γCO ₂	775	775	q ₃₀ , q ₂₈ , q ₂₆	13	22	22	30	2
δCO ₂	640	635	q ₃₁	4	3	-8	0	1
ξCO ₂	527	625	q ₂₅ , q ₂₈ , q ₁₁ , q ₃₀	6	8	25	11	3
τNH ₃	477	528	q ₂₉ , q ₁₁ , q ₂₅ , q ₂₇	42	35	-20	-19	4
δskel	399	432	q ₂₇	26	19	22	26	1
τCH ₃	296	355	q ₂₅ , q ₂₉ , q ₂₆	55	42	-33	-34	1
δskel	283	290	q ₂₆ , q ₂₉	9	10	50	48	0
δskel	219	264	q ₃₃ , q ₂₆	5	6	-30	-30	0
τCO ₂	184	170	q ₃₂	7	7	-9	-8	1

^a Reference 27. ^b B3LYP/6-31G* Onsager model optimized geometries and Hessians, frequencies in cm⁻¹. ^c B3LYP/6-31G* APT, A_i in km/mol. ^d RHF/6-311+G** APT, A_i in km/mol. ^e B3LYP/6-31G* APT and RHF/6-31G** distributed origin gauge AAT, R_i are in units of esu² cm² × 10⁴⁴. ^f RHF/6-311+G** APT and RHF/6-31G** distributed origin gauge AAT, R_i are in units of esu² cm² × 10⁴⁴. ^g RHF/6-311+G** polarizability derivatives.

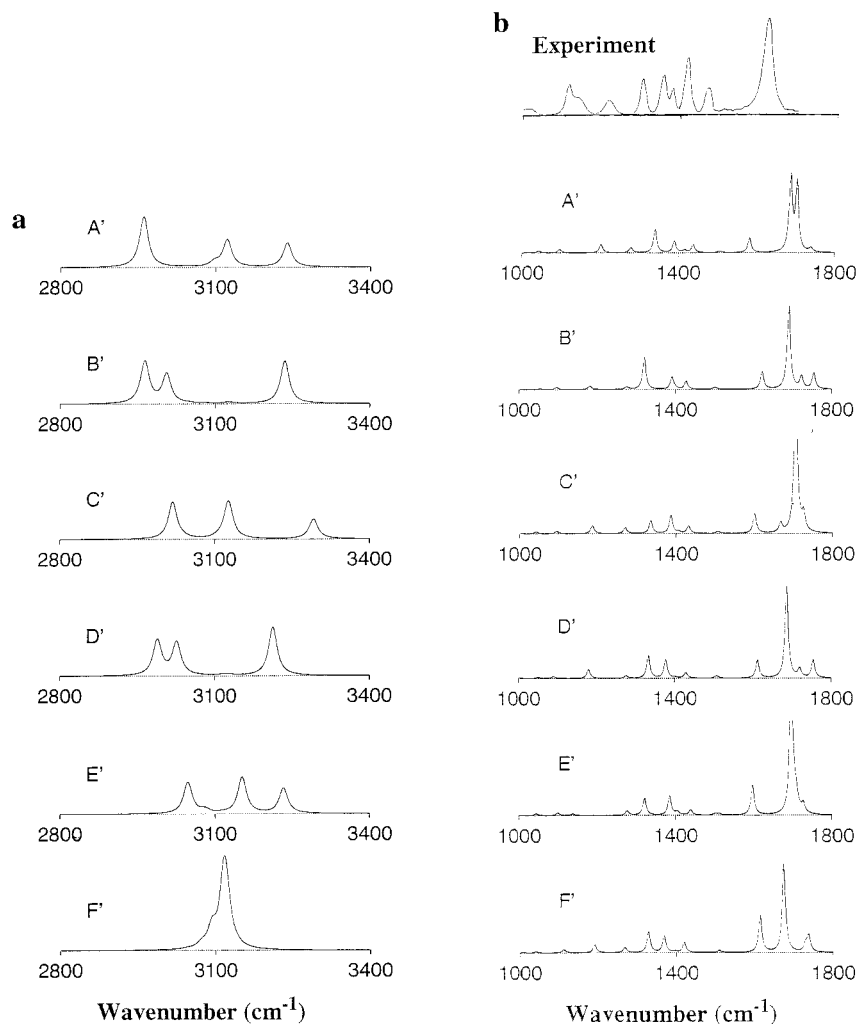


Figure 4. (a) Vibrational absorption spectra in the 3400–2800 cm⁻¹ region for different complexes of ALAZW and four water molecules calculated at B3LYP/6-31G*/Onsager model optimized geometries and using B3LYP/6-31G* APT. Absorption intensities are presented in km/mol. (b) Vibrational absorption spectra in the 1800–200 cm⁻¹ region for different complexes of ALAZW and four water molecules, calculated at B3LYP/6-31G*/Onsager model optimized geometries and using B3LYP/6-31G* APT. Absorption intensities are presented in km/mol. Experimental spectra are taken from ref 29.

the ALAZW are the same. In aqueous solution at room-temperature one would expect a distribution of various water positions which is changing with time.

In aqueous solution, the structure of the ALAZW is very much influenced by the surrounding solvent molecules, and the spectra are expected to be strongly influenced by the formation of strong hydrogen bonds. Therefore, the spectra obtained in aqueous solution in this region is probably a mixture of all of these modes (possibly more), which is consistent with the well known broad absorption of NH₃⁺ stretching modes in this region. In Table 1 one can see that in all cases, because of the different arrangement of the water molecules involved in the hydrogen bonding with the solute, we get different bond lengths for the three N–H bonds. Therefore, we do not expect to have asymmetric and symmetric stretching modes which originate from the equal stretch force constants for the three N–H bonds in the ammonium group. This result is different from the picture which is generally used for the interpretation of the N–H stretch modes in the NH₃⁺ group. Only a very slight change in the position of the water molecules in the first hydration shell may perturb the frequencies of the NH₃⁺ modes.

The absorptions of CH and CH₃ groups are, on the other hand, expected not to be influenced very much by the changes in the position of the surrounding water molecules. From the data in

Table S1 it can be seen that independently of the positions of the neighboring solvent molecules, the CH₃ stretching modes (q₄, q₅, and q₆) absorb at nearly the same frequencies in the different structures, even in the case of conformer F' which can be basically considered to be different from the other ones. These modes are coupled with each other and, contrary to the NH₃⁺ stretching modes, can be defined as two asymmetric and one symmetric stretching modes of the CH₃ group. The asymmetric CH₃ stretching modes absorb at 3149–3167 cm⁻¹ and 3125–3140 cm⁻¹, respectively, while symmetric stretching is predicted to absorb at frequencies ranging between 3058–3072 cm⁻¹ in the different conformers. Again, contrary to the NH₃⁺ group, the calculated splitting between the frequencies of the asymmetric stretching modes of methyl group is comparable to the experimental values.

Because of its hydrophobic nature, the methyl group does not have any direct contact with the solvent molecules. Actually, the high hydrophobic character of the methyl group is one of the most important problems we encountered during the further hydration of the ALAZW. In all cases the water molecules gather together at the hydrophilic side of the molecule (NH₃⁺ and COO⁻ groups) and the other side of the molecule cannot be easily encircled into the hydration shell. In order to completely surround the solute, one has to apply a very large

number of explicit solvent molecules, a factor which makes some parts of the calculations much more expensive. The CH₃ stretching modes (q_4 , q_5 , and q_6) are more or less independent of the conformer. The calculated frequencies for different conformers are very close to each other. However, these modes generally show low VA intensities, a fact arising from the apolar nature of the methyl group.

The methine (CH) stretching mode (q_7) is independent of the water positions and can be assigned in conformers **A'**–**F'** to the band at about 3110 cm⁻¹ (between 3093 cm⁻¹ in conformer **F'** and 3133 cm⁻¹ in conformer **C'**) (Table S1).

The next three calculated vibrational frequencies (in the region between 1600–1800 cm⁻¹) are C–O stretching modes (q_8 , q_9) which are coupled with the asymmetric NH₃⁺ deformations (q_{14} , q_{15}). These modes have large intensities and show significant differences between different conformers. In contrast to the asymmetric NH₃⁺ deformations (q_{14} , q_{15}), the symmetric NH₃⁺ deformation (q_{13}) is not coupled with the other modes. This mode is expected to be influenced by different arrangements of H-bonded water molecules and varies from 1602 cm⁻¹ for conformer **A'** to 1642 cm⁻¹ for conformer **B'** and shows a high intensity (Table S1).

Among the other modes which can be well assigned are the CH₃ asymmetric (q_{19} and q_{20}) and symmetric (q_{18}) deformations. The asymmetric CH₃ deformations are predicted to have low VA intensities and occur in the region between 1520 and 1536 cm⁻¹ for all conformers. The splitting between the asymmetric CH₃ deformations is less than 10 cm⁻¹ in all conformers. The symmetric CH₃ deformation (q_{18}), on the other hand, shows a larger intensity and is located at about 1450–1460 cm⁻¹ for conformers **A'**–**E'** while it occurs at 1441 cm⁻¹ for the **F'** conformer (Tables S1 and 4). This mode is strongly coupled with methine and NH₃⁺ rocking modes in the different conformers. Except for the q_{31} , q_{32} , and q_{33} vibrations, which are related to the torsion angles of the backbone and can be straightforwardly assigned, the other modes of the spectra are strongly coupled with each other and cannot be easily analyzed.

Because of the inclusion of explicit solvent molecules, the spectra are predicted to be significantly different with respect to the vibrational modes of the NH₃⁺ and CO₂⁻ groups in different conformers. The methyl group modes are not expected to be significantly influenced by the presence of water molecules in the present study. The calculated frequencies and splitting in this case are in good agreement with experimental values. For example, the asymmetric CH₃ deformations in conformer **A'**, calculated at 1527 and 1528 cm⁻¹, show a splitting of only 1 cm⁻¹ which is in agreement with experimental data (Table S1).

In Tables S1 and 4, we have also presented the VA intensities calculated using the RHF/6-311+G** APT. Although the overall predicted shape of the spectra seems to be the same for the different levels of theory (RHF/6-311+G** or B3LYP/6-31G*) for the APT calculations, there are a few vibrations whose intensities are significantly influenced by the level of calculation. The vibrational modes which are rather sensitive to the APT values and their intensities are influenced in this way are related to, or have a component of, the vibrational modes of NH₃⁺ or CO₂⁻ groups. Whether the direct involvement of these groups in the H-bond interaction of the solute and water molecules has any relation to this finding requires for more studies. In most cases, however, the intensities calculated on the basis of different APT values (from DFT or RHF calculations) are not significantly different and the predicted spectra would have a very similar shape.

The strong absorptions are related to the highly polar groups NH₃⁺ and CO₂⁻ whose local structural changes can significantly change the electric dipole derivatives. Since the arrangement of the water molecules and the local structural properties of these groups are mutually affected and since all of the studied different conformers in this study are energetically accessible in aqueous solution, the experimental results for the vibrations related to these groups are probably the average or the additive effect of a number of different conformers. This can clearly be observed from the broad shape of the NH₃⁺ absorption in the reported experimental results for the solution phase of the ALAZW.

In Table S2 (Supporting Information) the predicted VA spectra for six ALAZW stabilized by four water molecules calculated without application of the Onsager model are presented. The geometry, Hessian, and APT are calculated at B3LYP/6-31G* level of theory. In case of a few normal modes, both frequencies and absorption intensities are different from the corresponding values from Onsager model optimized structures. These vibrational modes which are sensitive to the presence of the continuum model are related to the NH₃⁺ or CO₂⁻ groups. Examination of the optimized geometries in two models (with or without Onsager model) (Table 1) clearly shows that the polar groups are significantly influenced after inclusion of the continuum model in the calculations. This effect can be explained by the polar nature of these groups, on one hand, and, more importantly, H-bond formation with the water molecules which can be affected by further hydration effects. Therefore, the corresponding normal modes are also expected to be influenced after inclusion of further solvation effects.

VCD Spectra. In this section we report the calculated VCD spectra for the conformers **A'**–**F'**. In the previous section we showed that the calculated VA spectra of the conformers are significantly influenced by the presence and the position of the explicit water molecules. Here we compare the predicted VCD spectra for the investigated conformers and study the differences between the predicted spectra caused by the different arrangements of the ALAZW and the four water molecules. In Table S3 (Supporting Information) we report the calculated VCD spectra for our six ALAZW conformers stabilized by four water molecules and the Onsager reaction field model (**A'**–**F'**). The high frequency and mid-IR regions of the VCD spectra for six conformers are depicted in Figure 5a and b, respectively. The calculated VCD spectra for the most energetically favorable conformer, conformer **F'**, are also presented in Table 4.

Experimental VCD spectra for alanine in aqueous solution have been reported in the 1500–1000 cm⁻¹ region. Because of the strong absorption of water between 1550 and 1700 cm⁻¹, the region is masked and is inaccessible in VCD experiments performed in normal water. There is a significant difference in the 1700–1800 cm⁻¹ region between the **F'** conformer, which has a different structure for ALAZW solute, and the other conformers. Conformer **F'** shows significantly lower intensities for the VCD absorption in this region (Table 4 and Figure 5b). There are, however, completely different patterns of positive and negative signs for the other conformers (**A'**–**E'**) in this region. As has already been discussed in the previous section, the presence of water molecules can perturb the ALAZW such that the calculated vibrational frequencies, potential energy distributions, intensities, and relative orders for charged chemical groups differ significantly. Therefore, depending on the position of the water molecules in the complex structure, the pattern of positive–negative alternation in the calculated spectra of the various conformers could be different, causing the calculated

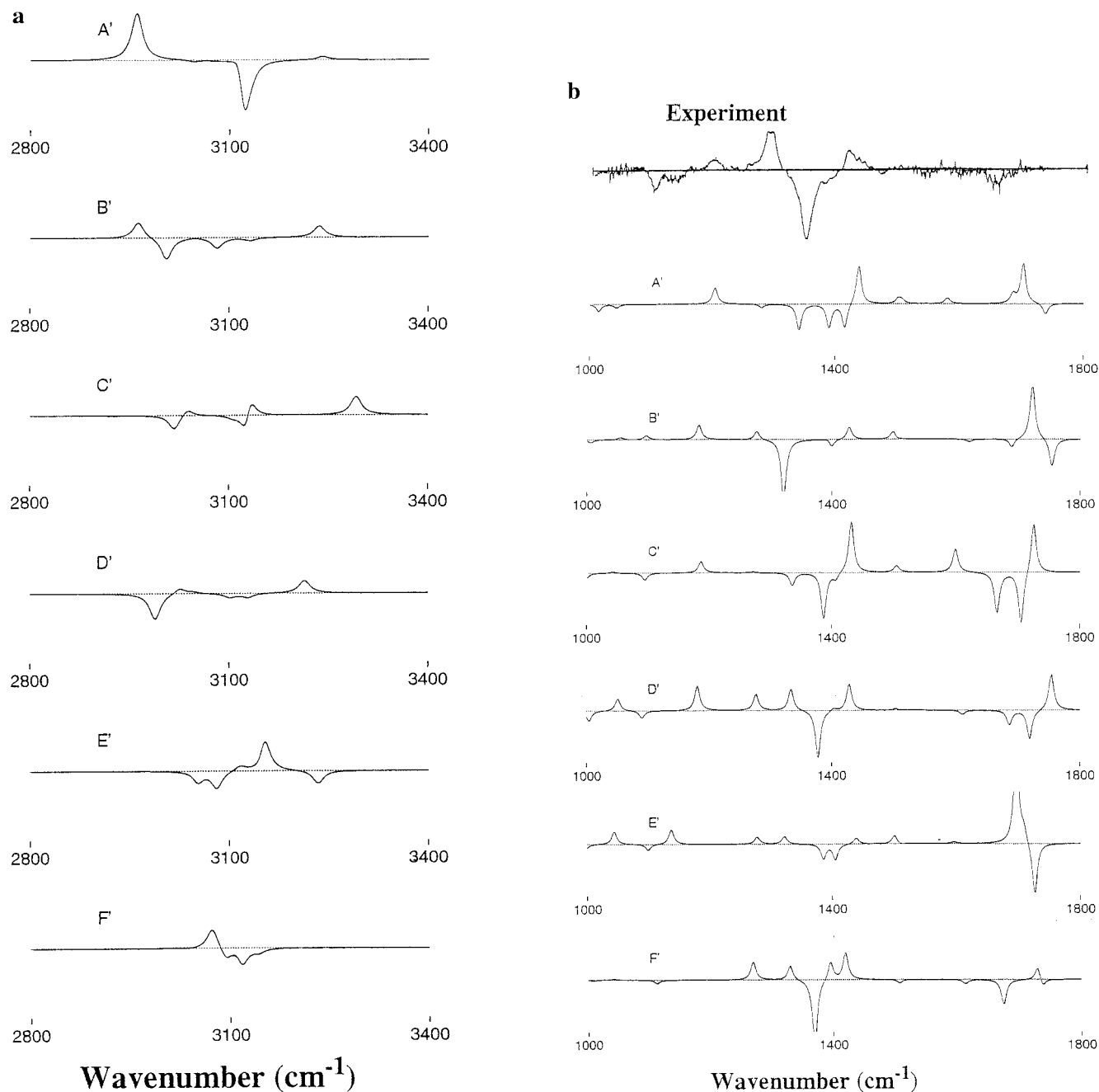


Figure 5. (a) VCD spectra in the 3400–2800 cm^{-1} region for different complexes of ALAZW and four water molecules, calculated at B3LYP/6-31G*/Onsager model optimized geometries and using B3LYP/6-31G* APT and RHF/6-31G** distributed origin gauge AAT. Absorption intensities are presented in units of $\text{esu}^2 \text{cm}^2 \times 10^{44}$. (b) VCD spectra in the 1800–200 cm^{-1} region for different complexes of ALAZW and four water molecules, calculated at B3LYP/6-31G*/Onsager model optimized geometries and using B3LYP/6-31G* APT and RHF/6-31G** distributed origin gauge AAT. Absorption intensities are presented in units of $\text{esu}^2 \text{cm}^2 \times 10^{44}$. Experimental spectra are taken from ref 29.

spectra average to zero or be drastically reduced. Consideration of the large coupling of these modes makes the situation more complicated.

In Tables 4 and S3, we have also presented the VCD intensities calculated using the RHF/6-311+G** APT and distributed origin gauge AAT. Similar to the VA spectra, the overall shape of the VCD spectra is the same using the different APTs. Regarding the effect of the level of APT calculation on the predicted spectra, very small changes in the intensities of the vibrational modes can be observed in VCD spectra as compared to the VA spectra (Tables 4 and S3).

In Figure 5b, we compared the simulated VCD spectra of different conformers with the experimental data.²⁹ In the case of all conformers, large negative absorption can be seen between

1350 and 1400 cm^{-1} . This negative absorption corresponds to the vibrational frequencies of 1361–1436 cm^{-1} , 1341 cm^{-1} , 1356–1427 cm^{-1} , 1398 cm^{-1} , 1406–1426 cm^{-1} , and 1390 cm^{-1} for conformers A'–F', respectively (Table S3). Examination of the potential energy distributions presented in Table 4 reveals that the C_α -H rocking modes (q_{23} and q_{24}) and the CO_2^- stretching normal modes (q_8 and q_9) contribute to the absorption at the above-mentioned frequencies in different conformers. The large negative absorption in the simulated VCD spectra corresponds to the intense negative absorption at 1358 cm^{-1} in the experimental spectra.²⁹ This band is assigned by Diem et al.²⁹ to the methine deformation mode.

The simulated VCD spectra of the conformer F' (Table 4) shows the best agreement with the experimental spectra. For

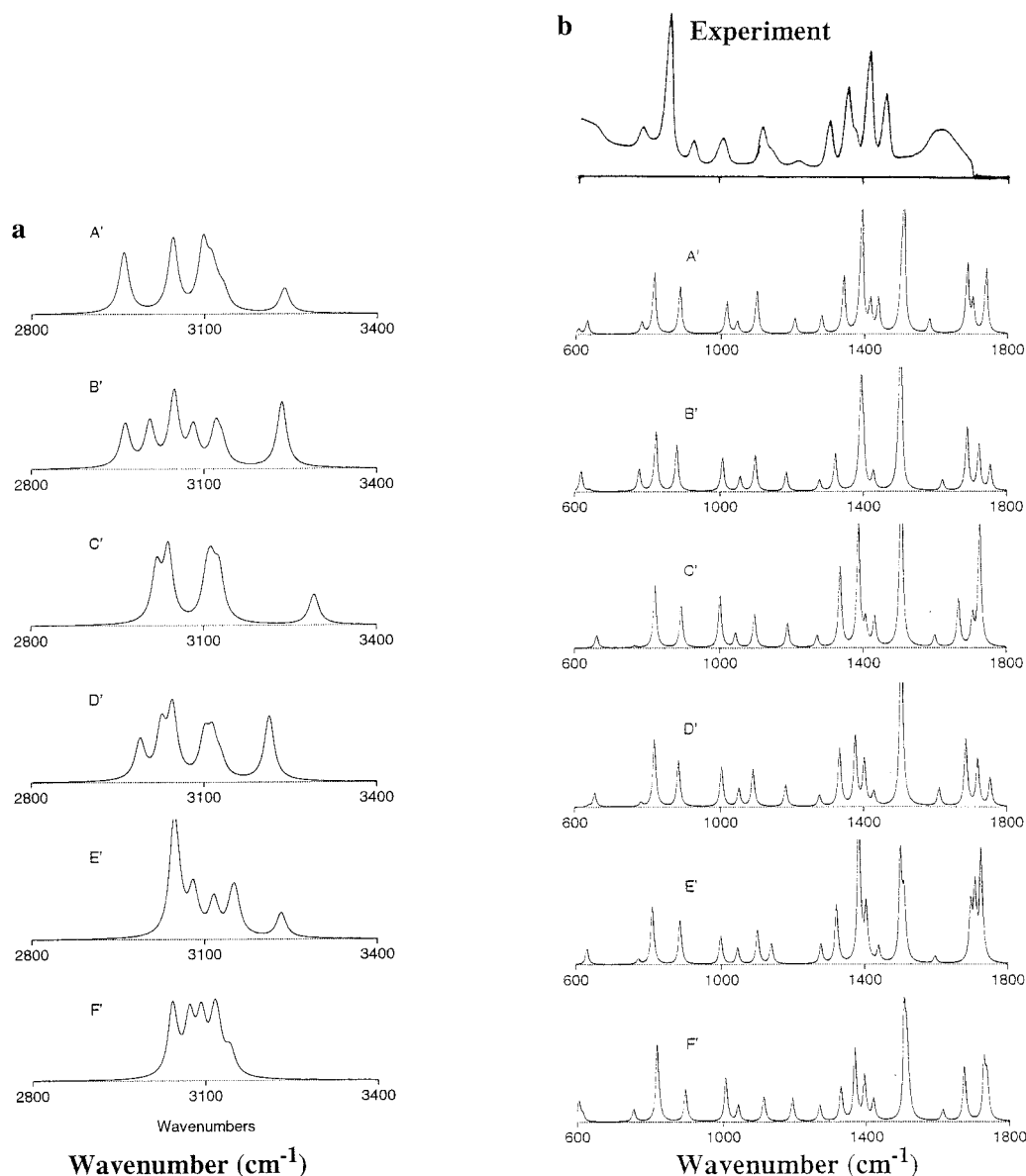


Figure 6. (a) Raman spectra in the 3400–2800 cm^{-1} region for different complexes of ALAZW and four water molecules, calculated at B3LYP/6-31G*/Onsager model optimized geometries and using RHF/6-311+G** polarizability derivatives. Absorption intensities are presented in $\text{\AA}^4/\text{amu}$. (b) Raman spectra in the 1800–600 cm^{-1} region for different complexes of ALAZW and four water molecules, calculated at B3LYP/6-31G*/Onsager model optimized geometries and using RHF/6-311+G** polarizability derivatives. Absorption intensities are presented in $\text{\AA}^4/\text{amu}$. Experimental spectra are taken from ref 20.

the conformer **F'** the relative intensities in the 1600–1800 cm^{-1} region and in the 1300–1500 cm^{-1} region of the simulated VCD spectra match the corresponding experimental spectra better than the simulated spectra of the other conformers. In the 1300–1500 cm^{-1} region we have much larger intensities in the VCD spectra, as compared to the absorptions in the 1600–1800 cm^{-1} region, in both the simulated spectra for the conformer **F'** and experimental data. The alternation of positive and negative peaks in the VCD spectra of conformer **D'** is also comparable to the experimental data. Conformer **F'** is the most energetically favorable cluster of ALAZW and four water molecules after including the Onsager continuum model to the B3LYP/6-31G* level geometry optimization. Compared to the spectra simulated using the optimized geometries of the ALAZW and four water molecules without the inclusion of the Onsager model (data not shown), inclusion of the solvation effects by application of a continuum model has improved the obtained results, significantly.

Polarized Raman Spectra. In Table S4 we present our polarized Raman predictions for the six conformers and show the simulated spectra in Figure 6a (high frequency region, 3400–2800 cm^{-1}) and 6b (mid-IR, 1800–600 cm^{-1}). The calculated polarized Raman spectra for the most energetically favorable conformer, conformer **F'**, are also compiled in Table 4.

As compared with the calculated VA and VCD spectra, the overall shape of the polarized Raman spectra seems to be less sensitive to the different arrangements of the water molecules included in the calculation. The polarized Raman spectra of all conformers have been simulated using electric dipole–electric dipole polarizability derivatives calculated at RHF/6-311+G** level of theory. The necessity of application of polarization functions in the basis set in the calculation of electric dipole–electric dipole polarizability derivatives for properly simulating the Raman spectra has been previously described.^{47–49}

For all studied structures, there are strong absorptions in the high frequency region of the spectra (Figure 6a). Because of

the lack of experimental data in this region, comparison could be performed only among the conformers. Similar to the high frequency (2800–3400 cm^{-1}) region of VCD and IR spectra, most of the differences in the shape of the polarized Raman spectra in this region can be related to the NH_3^+ stretching modes which, depending on the conformer and the relative position of water molecules, absorb at different frequencies.

In the mid-IR region, where the experimental data are available,^{20,27} the calculated spectra for different conformers have been aligned with the experimental spectra (Figure 6b). In this region the spectra of all conformers seem to be comparable with the experiments. In the 750–1250 cm^{-1} region of the experimental Raman spectra^{20,27} the most intense band can be observed at 850 cm^{-1} . This band was assigned by Diem et al.²⁷ to the symmetric stretching mode of C–N bond. As it was mentioned before, in this region (750–1250 cm^{-1}) there is a large coupling between different modes in different vibrational frequencies. Nevertheless, the frequencies of 906, 900, 914, 906, 908, and 918 cm^{-1} are calculated to have the largest contribution from the symmetric stretching mode of C–N bond (q_{10}) in conformers $\text{A}'\text{--F}'$, respectively. For these vibrational frequencies, relatively large intensities are calculated for the Raman polarized spectra. However, in our calculation, the most intense band in this region of the Raman spectra corresponds to the vibrational absorptions at 834, 842, 841, 839, 831, and 840 cm^{-1} , in conformers $\text{A}'\text{--F}'$, respectively (Table S1). These vibrations can be best assigned to the CO_2^- symmetric deformation which is largely coupled with other normal modes, like the C–N and $\text{C}_\alpha\text{--C}'$ stretching modes, in different conformers.

The experimental bands at 1301 and 1351 cm^{-1} were assigned by Diem et al.²⁷ to the $\text{C}_\alpha\text{--H}$ bending modes. However, there must be significant contributions from the NH_3^+ bending motions because these bands shift to 1291 and 1337 cm^{-1} , respectively, upon deuterating the NH_3^+ group. The calculated vibrations at 1300 and 1361, 1297 and 1341, 1291 and 1356, 1297 and 1354, 1298 and 1342, and 1298 and 1350 cm^{-1} , for conformers $\text{A}'\text{--F}'$, respectively, have significant mixing of $\text{C}_\alpha\text{--H}$ rocking modes (q_{23} and q_{24}) and NH_3^+ bending motions (q_{16} , q_{17}) (Table S1). Therefore, assigning these calculated vibrational absorptions to the two experimental bands at 1301 and 1351 cm^{-1} seems reasonable. Comparison of the calculated frequencies in this region with the experimentally assigned frequencies also indicates that unscaled DFT results are quite promising with respect to the reproduction of the experimental frequencies.

On the basis of isotopic data, the experimental Raman bands at 1375 and 1459 cm^{-1} were assigned by Diem et al.²⁷ to methyl deformations. The 1375 cm^{-1} band is due to the symmetric methyl bending mode. This band correlates with the absorptions at 1436, 1448, 1452, 1449, 1460, and 1441 cm^{-1} , for conformers $\text{A}'\text{--F}'$, respectively (Table S1). The 1459 cm^{-1} band in the experimental spectra is due to the nearly degenerate pair of antisymmetric methyl bending modes. These modes can be well correlated with the calculated antisymmetric methyl bending modes (q_{19} and q_{20}) absorbing for conformers $\text{A}'\text{--F}'$ at 1523 and 1529, 1520 and 1525, 1526 and 1528, 1527 and 1528, 1522 and 1523, and 1529 and 1536 cm^{-1} , respectively (Table S1). The calculated splitting between the antisymmetric methyl bending modes are less than 10 cm^{-1} in case of all of the conformers.

The experimental Raman band at 1410 cm^{-1} is assigned to the symmetric CO_2^- stretching mode.²⁷ In our calculations the second mode which can be assigned to the CO_2^- stretching can

be observed at 1410, 1412, 1407, 1398, 1406, and 1390 cm^{-1} frequencies for the conformers $\text{A}'\text{--F}'$, respectively (Table S1). These CO_2^- stretching modes are, however, strongly coupled with other normal modes in different conformers (Table S1). For the Raman spectra of all conformers, large intensities are predicted for these frequencies, respectively. This is in complete agreement with the intense peak which can be observed in the experimental spectra.

For appropriate assignment of stretching modes of the CO_2^- group to one asymmetric and one symmetric stretching modes, the bond distances of the two C–O bonds should be equal. Therefore, in cases where we do not have equal bond distances for the C–O bonds, we may not get the expected contributions of two C–O bond stretching modes (q_8 and q_9 in the present study) to the assigned frequencies. With this respect, in the case of conformers A' , C' , and E' , where the C–O bond lengths are approximately equal to each other (Table 1), we observe the significant contribution of both q_8 and q_9 stretching modes in the two CO_2^- stretching vibrations (Table S1). In conformers B' , D' , and F' , on the other hand, where these two bonds have significantly different bond distances, either q_8 or q_9 stretching modes contribute to the second stretching mode of the CO_2^- group absorption and, therefore, the band cannot be properly considered as a symmetric stretching mode (Table S1).

The difficulties in the proper assignment of the symmetric stretching mode of the CO_2^- group, as compared to the experiments, have been reported in previous studies.²⁰ In the previous investigations, the ALAZW has been studied in the absence of explicit water molecules and at the RHF level of theory. In this way the most energetically favorable conformer of ALAZW is the HO conformer (Figure 2). In this conformer, because of the presence of a strong intramolecular H-bond between one of the oxygen atoms of the CO_2^- group and one of the hydrogen atoms in the NH_3^+ group, there is a pronounced difference between the bond distances of the two C–O bonds. In conformer HHOO (Figure 2) which is only stable in the presence of explicit water molecules the relative orientation of the two oxygen atoms with respect to the NH_3^+ group is more symmetric. The explicit water molecules which are used to stabilize the ALAZW and the pattern and strength of their hydrogen bonds can be significantly influenced by the presence of further hydration shells. Therefore, the presence of only four water molecules in the environment of the ALAZW results in different possible hydrogen bonded clusters which, at least with respect to the bond distances in the NH_3^+ and CO_2^- groups, are totally different from each other. This can be clearly observed in the case of conformers B' , D' , and F' . With this respect, although application of a continuum model may improve the results, inclusion of a sufficient number of water molecules in the calculations would be the best approach to overcome this difficulty.

Conclusions

The potentially large influence of the solvent environment on the structural and other properties of molecules in solution is well known to be of significant importance in the study of chemical and biochemical events. However, in most studies, because of the large expense of the calculations introduced by either implicit or partially explicit inclusion of solvent molecules and/or complexity of the different possible arrangements of such solvent molecules, the solvation effects have been ignored and the system has been modeled by the gas phase approximation. There are a few successful approaches in order to partly simulate the solvent effects by the application of the continuum models

in the calculations. Although these models are much closer to simulating the real environment of the solute than gas phase calculations, they mostly approximate the solvent effect by the overall electrostatic field of the solvent and do not include explicit interactions between the solvent and the solute which are important, for example, in the case of the H-bond formation. Therefore, wherever such explicit interactions are absent, like simulation of organic solvents or simulation of non polar solutes they can be more successfully applied. In the case of water simulations one has to keep in mind that the application of such models is only able to describe the continuum effect of the surrounding water molecules on the solute system, that is, the bulk water effects. Specifically for systems such as the ALAZW, which is able to form strong hydrogen bonds with water molecules, one may expect significant differences between the implicit and explicit inclusion of the solvent environment. The results of the present study clearly indicate such differences. In contrast to all previous theoretical studies applying either pure gas phase calculations or implicit solvent inclusion which resulted in the HO conformer, we have shown that by including the explicit water molecules one can obtain completely different structures for the studied molecule. In the case of the ALAZW, which can also be considered as a reasonable model for other amino acids, these substantial differences in the structure are directly coupled with the two most important dihedral angles of the molecule. In polypeptide structures the carboxylate and ammonium groups of amino acids are involved in the formation of peptide bonds, and therefore, the obtained results of the present study should not be directly transformed to any conclusion about the prediction of secondary structures in protein structures. However, elucidation of the structural details of amino acids as the building units of protein structures seems to be essential for the better understanding of the structure and function of these macromolecules. We have also looked at the effects of adding explicit water molecules to a model compound for peptides and proteins, *N*-acetyl-L-alanine-*N'*-methylamide³⁸ and also the simple dipeptide L-alanyl-L-alanine.⁵⁴

The introduction of the water molecules into the calculations has large effects on the calculated structural preference of the solute and results in different optimized conformations for the ALAZW molecule as compared to the gas phase calculations of the isolated ALAZW molecule. The calculated spectra for these conformations of the ALAZW show reasonable agreement with the reported spectroscopical experimental data. However, the relative arrangement of the explicit water molecules around the solute molecule and the pattern and strength of hydrogen bonding of these water molecules with the solute as well as with other water molecules are extremely sensitive to the further hydration shells. The potential effect of further solvation effects can be partly simulated by inclusion of a continuum reaction field in the calculations. As was experienced in the present study, after application of the Onsager model the results show significant improvement. With respect to the simulation of the spectra, the inclusion or exclusion of the water molecules at different stages of the calculations such as geometry optimization and calculations of second derivatives and tensors can significantly influence the obtained results. The possibility of having more than one conformer in solution with different rearrangements of the water molecules should also be kept in mind. The introduction of a sufficient number of water molecules in the calculations may also be important. We believe that the major part of the observed differences in the calculated spectra for different conformers originate from the different arrangements of the water molecules in the vicinity of the solute. As

mentioned before, the presence of the second hydration shell may influence the structure, relative arrangement, and hydrogen bonding patterns of the solvent molecules in the first shell which in turn affect the structural properties of the solute. Because of these possible complications, we decided to include more water molecules into the calculation and study the effect of this consideration on the predicted structure and vibrational spectra of the ALAZW. These calculations are in progress in this laboratory. We are also investigating the Raman optical activity for a number of conformers which can be helpful for comparing the calculated structural data with experiments.

The results of the present study on the structure of the ALAZW clearly show that the inclusion of explicit water molecules in the calculations substantially influences the calculated structural and spectroscopic properties and hence the subsequent vibrational analyses of the studied molecules.

Acknowledgment. E.T. and K.J.J. would like to acknowledge receipt of a scholarship by the European Union for their support at the German Cancer Research Center. The authors would also like to thank H. Bohr at the Technical University of Denmark (Lyngby) for valuable discussions and for providing computing time on the SGI Power Challenge array at Aarhus University. The authors would like to thank Roger D. Amos and Nick C. Handy for providing us with the Cambridge Analytical Derivatives Package (CADPAC), which was used to calculate all of the distributed origin gauge atomic axial tensors in this paper.

Supporting Information Available: Tables of numerical data for vibrational absorption spectra of conformers $A'-F'$, vibrational absorption spectra of conformers $A-F$, VCD spectra of conformers $A'-F'$, and polarized Raman spectra of conformers $A'-F'$, respectively, (4 pages). Ordering information is given on any current masthead page.

References and Notes

- (1) Godfery, P. D.; Brown, R. D. *J. Am. Chem. Soc.* **1995**, *117*, 2019.
- (2) Godfery, P. D.; Firth, S.; Hatherley, L. D.; Brown, R. D.; Pierlot, A. P. *J. Am. Chem. Soc.* **1993**, *115*, 9687.
- (3) Iijima, K.; Tanaka, K.; Onamu, S. *J. Mol. Struct.* **1991**, *246*, 257.
- (4) Iijima, K.; Beagley, B. *J. Mol. Struct.* **1991**, *248*, 133.
- (5) Reva, I. D.; Stepanian, S. G.; Plokhotnichenko, A. M.; Radchenko, E. D.; Sheina, G. G.; Blagoi, Y. P. *J. Mol. Struct.* **1994**, *318*, 1.
- (6) Reva, I. D.; Plokhotnichenko, A. M.; Stepanian, S. G.; Ivanov, A. Y.; Radchenko, E. D.; Sheina, G. G.; Blagoi, Y. P. *Chem. Phys. Lett.* **1995**, *232*, 141.
- (7) Hu, C.-H.; Shen, M.; Schaefer, H. F., III. *J. Am. Chem. Soc.* **1993**, *115*, 2923.
- (8) Császár, A. G. *J. Mol. Struct.* **1995**, *346*, 141.
- (9) Császár, A. G. *J. Am. Chem. Soc.* **1992**, *114*, 9569.
- (10) Schäfer, L.; Siam, K.; Klimkowski, V. L.; Ewbank, J. D.; van Alsenoy, C. *J. Mol. Struct. (THEOCHEM)* **1990**, *63*, 361.
- (11) Schäfer, L.; Kulp-Newton, S. Q.; Siam, K.; Klimkowski, V. J.; van Alsenoy, C. *J. Mol. Struct.* **1990**, *209*, 373.
- (12) Cao, M.; Newton, S. Q.; Pranata, J.; Schäfer, L. *J. Mol. Struct. (THEOCHEM)* **1995**, *332*, 251.
- (13) Frey, R. F.; Coffin, J.; Newton, S. Q.; Ramek, M.; Cheng, V. K. W.; Momany, F. A.; Schäfer, L. *J. Am. Chem. Soc.* **1992**, *114*, 5369.
- (14) Ramek, M.; Cheng, V. K. W.; Frey, R. F.; Newton, S. Q.; Schäfer, L. *J. Mol. Struct. (THEOCHEM)* **1991**, *235*, 1.
- (15) Jensen, J. H.; Gordon, M. S. *J. Am. Chem. Soc.* **1991**, *113*, 7917.
- (16) Jensen, J. H.; Baldrige, K. K.; Gordon, M. *J. Phys. Chem.* **1992**, *96*, 8340.
- (17) Gronert, S.; O'Hair, R. A. J. *J. Am. Chem. Soc.* **1995**, *117*, 2071.
- (18) Godfrey, P. D.; Brown, R. D.; Rodgers, F. M. *J. Mol. Struct.* **1996**, *376*, 65.
- (19) Császár, A. G. *J. Phys. Chem.* **1996**, *100*, 3541.
- (20) Barron, L. D.; Gargaro, A. R.; Hecht, L.; Polavarapu, P. L. *Spectrochim. Acta* **1991**, *47A*, 1001.
- (21) Yu, G. S.; Freedman, T. B.; Nafie, L. A.; Deng, Z. Polavarapu, P. L. *J. Phys. Chem.* **1995**, *99*, 835.

- (22) Levy, H. A.; Corey, R. B. *J. Am. Chem. Soc.* **1941**, *63*, 2095.
- (23) Donohue, J. *J. Am. Chem. Soc.* **1950**, *72*, 949.
- (24) Takagi, S.; Chihara, H.; Seki, S. *Bull. Chem. Soc. Jpn.* **1959**, *32*, 84.
- (25) Junk, G.; Sevec, H. *J. Am. Chem. Soc.* **1963**, *85*, 839.
- (26) Lehmann, M. S.; Koetzle, T. F.; Hamilton, N. C. *J. Am. Chem. Soc.* **1972**, *94*, 2657.
- (27) Diem, M.; Polavarapu, P. L.; Oboodi, M.; Nafie, L. A. *J. Am. Chem. Soc.* **1982**, *104*, 3329.
- (28) Diem, M. *Introduction to Modern Vibrational Spectroscopy*; John Wiley & Sons: New York, pp 194–198 (section 7.5).
- (29) Diem, M. *J. Am. Chem. Soc.* **1988**, *110*, 6967.
- (30) Lal, B. B.; Diem, M.; Polavarapu, P. L.; Oboodi, M.; Freedman, T. B.; Nafie, L. A. *J. Am. Chem. Soc.* **1982**, *104*, 3336.
- (31) Stephens, P. J.; Devlin, F. J.; Chabalowski C. F.; Frisch, M. J. *J. Phys. Chem.* **1994**, *98*, 11623.
- (32) Devlin, F. J.; Stephens, P. J.; Cheeseman, J. R.; Frisch, M. J. *J. Am. Chem. Soc.* **1996**, *118*, 6327.
- (33) Stephens, P. J.; Devlin, F. J.; Ashvar, C. S.; Chabalowski C. F.; Frisch, M. J. *Faraday Discuss.* **1994**, *99*, 103.
- (34) Devlin, F. J.; Stephens, P. J.; Cheeseman, J. R.; Frisch, M. J. *J. Phys. Chem. A* **1997**, *101*, 9912.
- (35) Devlin, F. J.; Stephens, P. J.; Cheeseman, J. R.; Frisch, M. J. *J. Phys. Chem. A* **1997**, *101*, 6322.
- (36) Jalkanen, K. J.; Suhai, S. *Chem. Phys.* **1996**, *208*, 81.
- (37) Jalkanen, K. J.; Suhai, S.; Bohr, H. *Theoretical and Computational Methods in Genome Research*; Plenum Press: New York, 1997; pp 255–277.
- (38) Han, W.; Jalkanen, K. J.; Suhai, S. *J. Phys. Chem. B* **1998**, *102*, 2587.
- (39) Handy, N. C.; Murray, C. W.; Amos, R. D. *J. Phys. Chem.* **1993**, *97*, 4392.
- (40) Johnson, B. G.; Gill, P. M. W.; Pople, J. A. *J. Chem. Phys.* **1993**, *98*, 5612.
- (41) Florián, J.; Baumruk, V.; Štrajbl, M.; Bednárová, L.; Štěpánek, J. *J. Phys. Chem.* **1996**, *100*, 1559.
- (42) Florián, J.; Baumruk, V.; Leszczynski, J. *J. Phys. Chem.* **1996**, *100*, 5578.
- (43) Illich, P.; Hemann, C. F.; Hille, R. *J. Phys. Chem. B* **1997**, *101*, 10923.
- (44) *Insight II User Guide*, October 1995; Biosym/MSI: San Diego, 1995.
- (45) Frisch, M. J.; Trucks, G. W.; Schlegel, H. B.; Gill, P. M. W.; Johnson, B. G.; Robb, M. A.; Cheeseman, J. R.; Keith, T.; Peterson, G. A.; Ortiz, J. V.; Foresman, J. B.; Cioslowski, J.; Stefanov, B. B.; Nanayakkara, A.; Challacombe, M.; Peng, C. Y.; Ayala, P. Y.; Chen, W.; Wong, M. W.; Andres, J. L.; Replogle, E. S.; Gomperts, R.; Martin, R. L.; Fox, D. J.; Binkley, J. S.; Defrees, D. J.; Baker, J.; Stewart, J. P.; Head-Gordon, M.; Gonzales, C.; Pople, J. A. *Gaussian 94*, Revision C.3; Gaussian, Inc.: Pittsburgh, PA, 1985.
- (46) Frisch, M. J.; Yamaguchi, Y.; Gaw, J. F.; Schaefer, H. F., III; Binkley, J. S. *J. Chem. Phys.* **1986**, *84*, 531.
- (47) Amos, R. D. *Chem. Phys. Lett.* **1986**, *124*, 376.
- (48) Amos, R. D. In *Ab Initio Methods in Quantum Chemistry*; Lawley, K. P., Ed.; Wiley: New York, 1987.
- (49) Johnson, B. G.; Florian, J. *Chem. Phys. Lett.* **1995**, *247*, 120.
- (50) Kormonicki, A.; McIver, J. W., Jr. *J. Chem. Phys.* **1979**, *70*, 2014.
- (51) Ding, Y.; Krogh-Jespersen, K. *Chem. Phys. Lett.* **1992**, *199*, 261.
- (52) Yu, D.; Armstrong, D. A.; Rank, A. *Can. J. Chem.* **1992**, *70*, 1792.
- (53) Pulay, P.; Fogarasi, G.; Pang, F.; Boggs, J. E. *J. Am. Chem. Soc.* **1979**, *101*, 2550.
- (54) Jalkanen, K. J.; Knapp-Mohammady, M.; Suhai, S.; Bohr, H.; Nardi, F.; Wade, R. C. To be published.